ANALYSIS OF DYNAMIC STRESS INTENSITY FACTORS FOR CRACKED STIFFENED PLATES BASED ON EXTENDED FE METHOD

(DOI No: 10.3940/rina.ijme.2020.a1.547)

Y Peng Departments of Naval Architecture, Ocean and Structural Engineering, School of Transportation, Wuhan University of Technology, China and **P Yang**, Key Laboratory of High Performance Ship Technology of Ministry of Education (Wuhan University of Technology), and Departments of Naval Architecture, Ocean and Structural Engineering, School of Transportation, Wuhan University of Technology, China

SUMMARY

The dynamic stress intensity factors (DSIFs) for cracked stiffened plates considering the actual boundary conditions in ship structures are analyzed by the extended finite element method (XFEM). The sensitivity of numerical results with respect to mesh size and time step is discussed. Some other influential parameters including stiffener height, crack location and crack length are also analyzed. The numerical results show that the convergence is affected by mesh size and time step. By using XFEM, singular elements are not needed at the crack front and moderately refined meshes can achieve good accuracy. The height of the stiffener and crack location significantly effect DSIFs, while the crack length slightly influences the DSIFs.

NOMENCLATURE

$H(\boldsymbol{x})$	Heaviside step function (Moës *et al*., 1999)
$F_l(\boldsymbol{x})$	Westergaard asymptotic function (Moës *et al*., 1999)
ϕ	Nodal shape function
$\boldsymbol{u}^h$	Nodal displacement vector
K_s	Static stress intensity factors (MPa m$^{1/2}$)
$K_I(t)$, $K_{II}(t)$	Mode I, Mode II dynamic stress intensity factors (Moës *et al*., 1999)
c	Half crack length (mm)
W	Half width of finite plate (mm)
H	Half height of finite plate (mm)
a	Length of plate (mm)
b	Width of plate (mm)
t_p	Thickness of plate (mm)
h_w	Height of stiffener (mm)
t_w	Thickness of stiffener (mm)

1. INTRODUCTION

The environmental loadings on ships and offshore structures in rough sea or emergencies, such as impact and earthquake, should be considered as dynamic loads. When a cracked structure is subjected to dynamic loading, the load is propagated by stress waves. Thus, the interaction between the stress waves and cracks makes the dynamic fracture more complex than in quasi-static cases. As the basic components of ships and offshore structures, stiffened steel plates are widely used because of their light-weight, high structure efficiency and good crack arresting properties. In hull structures cracking damage is typically initiated in welded or stress concentration regions, such as the intersection line between plate and stiffener. These cracks may grow under dynamic loading conditions, resulting in cracks of various sizes, locations and orientations. Therefore, an important task is to accurately evaluate the dynamic stress intensity factors (DSIFs) for cracked stiffened plates. These can then be used to investigate crack initiation, propagation and arrest under dynamic loading.

Chen (1975) examined a centrally cracked rectangular finite strip subjected to step loading using a Lagrangian finite difference method. DSIFs were obtained from the relation between DSIFs and stress fields in the vicinity of the crack tip. This problem has been considered as a benchmark and examined by many researchers. Lin and Ballmann (1993) reconsidered Chen's problem using the same method. Their numerical results are almost identical with those obtained by Chen except for a few time periods when wave fluctuations occurs. Song and Paulino (2006) evaluated DSIFs for both homogeneous and non-homogeneous materials by using the interaction integral method. Xie *et al*. (2007, 2009) calculated DSIFs for some dynamic stationary cracks based on the virtual crack closure technique (VCCT). By using the implicit time scheme, the results obtained are in good agreement with the benchmark (Chen, 1975) results. Nevertheless, among the existing research, the mesh dependence of the crack is one of the main drawbacks.

The partition of unity method (PUM) for discontinuities and near-tip crack fields was firstly introduced by Belytschko and Black (1999). The name XFEM was given by Moës *et al*. (1999) and Dolbow *et al*. (2000) after proposing two types of nodal enrichments to model the crack. The nodes of fully-cut elements are enriched by the Heaviside step function, while the Westergaard asymptotic function is used to enrich the nodes of the elements containing the crack tips. Sukumar *et al*. (2000) described three-dimensional crack modelling by XFEM and stress intensity factors (SIFs) for planar three-dimensional cracks were presented. Because of modeling of the discontinuities without any dependence with the mesh size and orientation, XFEM has more advantages than classical finite element method (FEM) in dealing with fracture problems. In recent years, more and more researchers have adopted XFEM approaches to analyse

discontinuous phenomena occurring in structures under quasi-static (González-Albuixech *et al*., 2013; Qian *et al*., 2016; Bergara *et al*., 2017; Kumar *et al*., 2017; Wang *et al*., 2017; Feng & Li, 2018) or dynamic loading (Nistor *et al*., 2008; Menouillard *et al*., 2010; Haboussa *et al*., 2011; Saribay & Nied, 2014; Agarwal *et al*., 2015; Wen & Tian, 2016). However, the relevant investigations have been largely limited to specimens and benchmark problems. Because of this complexity, few researchers have considered dynamic fracture problems in actual engineering structures (Chen & Chen, 2013; Shimbo, 2017). Literature on dynamic fracture research using XFEM does not seem to be available for the stiffened plates in ship hull structures.

In the present paper, XFEM is adopted to calculate the DSIFs for stiffened plates with a central crack in the plate. Actual boundary conditions for cracked stiffened plates in ship structures are considered. In order to verify the reasonability, both 2D and 3D models are compared by means of FEM and XFEM in a benchmark problem. Then the DSIFs for cracked stiffened plates are evaluated by XFEM. The sensitivity of numerical results with respect to mesh size and time step is discussed. The influences of stiffener height, crack length and crack location are also considered in the analyses. Some meaningful conclusions on DSIFs for cracked stiffened plates are obtained from the study.

2. DEVELOPMENT OF XFEM

Based on the partition of unity method (PUM), XFEM incorporates a discontinuous function and the near-tip asymptotic fields to the standard displacement-based finite element approximation. For example, for the discretization shown in Figure 1 (in which squared nodes are enriched with the Heaviside function and have two additional degrees of freedom, while circled nodes are enriched with the crack tip functions and have eight additional degrees of freedom), the displacement approximation for two-dimensional crack modeling in XFEM takes the form due to Moës *et al*. (1999):

$$\boldsymbol{u}^h = \sum_{i\in I} \boldsymbol{u}_i \phi_i + \sum_{j\in J} \boldsymbol{b}_j \phi_j H(\boldsymbol{x}) + \sum_{k\in K} \phi_k \left(\sum_{l=1}^{4} \boldsymbol{c}_k^l F_l(\boldsymbol{x})\right) \tag{1}$$

where I is the set of all nodes in the mesh, ϕ_i is the nodal shape function, and $\boldsymbol{u}_i$ is the standard degrees of freedom (DOFs) of node i ($\boldsymbol{u}_i$ represents the physical nodal displacement for non-enriched nodes only). The subsets J and K contain the nodes enriched with the generalized Heaviside function $H(\boldsymbol{x})$ or crack tip functions $F_l(\boldsymbol{x})$, respectively, and $\boldsymbol{b}_j$, $\boldsymbol{c}_k^l$ are the corresponding DOFs.

The stress intensity factors (SIFs) are extracted by the interaction integral method in XFEM. The coordinates are taken to be the local crack tip co-ordinates with the x_1-axis parallel to the crack faces, as shown in Figure 2. Under general mixed mode situations, the SIFs can be related to the J-integral using the following expression (Moës *et al*., 1999):

$$J = \frac{K_I^2}{E^*} + \frac{K_{II}^2}{E^*} \tag{2}$$

where E^* is defined in terms of material parameters E (Young's modulus) and ν (Poisson's ratio) as:

$$E^* = \begin{cases} E & \text{plane stress} \\ \frac{E}{1-\nu^2} & \text{plane strain} \end{cases} \tag{3}$$

To compute the stress intensity factors K_I and K_{II}, auxiliary fields have to be introduced. Then the interaction integral is derived from the application of the J-integral to a problem where two stress fields are involved, resulting in the following decomposition:

$$J^{(1+2)} = J^{(1)} + J^{(2)} + I^{(1,2)} \tag{4}$$

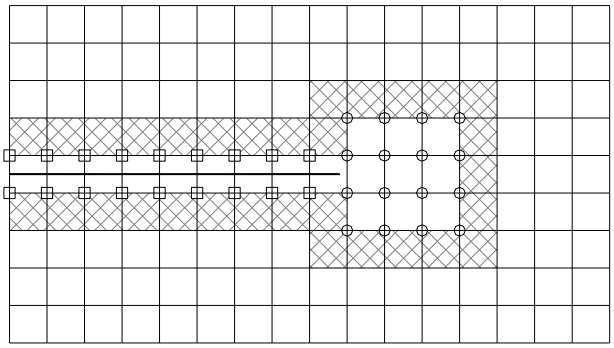

Figure 1 Enriched nodes for two-dimensional crack modeling in the XFEM

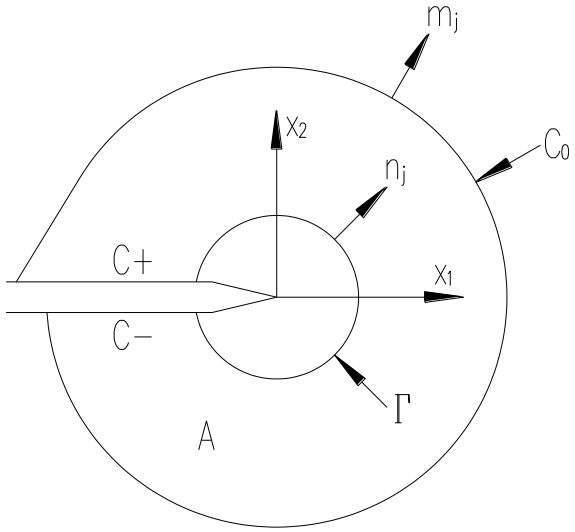

Figure 2 Schematic of the interaction integrals (Domain A is enclosed by Γ, C_+, C_-, C_0. Unit normal m_j=n_j on C_+, C_-, C_0, m_j=-n_j on Γ.)

The term $I^{(1,2)}$ corresponds to the interaction integral and includes the interaction between the two intervening fields, which may be written as

$$I^{(1,2)} = \int_{\Gamma}[W^{(1,2)}\delta_{1j} - \sigma_{ij}^{(1)}\frac{\partial(u_i^{(2)})}{\partial x_1} - \sigma_{ij}^{(2)}\frac{\partial(u_i^{(1)})}{\partial x_1}]\, n_j\, d\Gamma \quad (5)$$

where $(\sigma_{ij}^{(1)}, \varepsilon_{ij}^{(1)}, u_i^{(1)})$ corresponds to the actual state and $(\sigma_{ij}^{(2)}, \varepsilon_{ij}^{(2)}, u_i^{(2)})$, is an auxiliary state, which has to be chosen as the asymptotic fields for Mode I or II. $W^{(1,2)}$ is the interaction strain energy, and may be written as:

$$W^{(1,2)} = \sigma_{ij}^{(1)}\varepsilon_{ij}^{(2)} = \sigma_{ij}^{(2)}\varepsilon_{ij}^{(1)} \quad (6)$$

As contour Γ approaches the crack tip, the relationship between the interaction integral and the SIFs of the actual and auxiliary fields is:

$$I^{(1,2)} = \frac{2}{E^*}\left(K_I^{(1)}K_I^{(2)} + K_{II}^{(1)}K_{II}^{(2)}\right) \quad (7)$$

Substituting $K_I^{(2)} = 1, K_{II}^{(2)} = 0$ and $K_I^{(2)} = 0, K_{II}^{(2)} = 1$ into Eq. (7), respectively, Mode I and Mode II SIFs of actual fields can be decoupled and determined as:

$$K_I = \frac{E^*}{2}I^{(1)}, K_{II} = \frac{E^*}{2}I^{(2)} \quad (8)$$

3. METHOD VERIFICATION

In this section, a center cracked tension (CCT) specimen is analyzed to verify the XFEM implementation for comparison, which is a pure mode-I problem and was first studied by Chen (1975). Figure 3(a) shows a rectangular finite plate of width 2*W*=20 mm and height 2*H*=40 mm, with a central crack of length 2*c*=4.8 mm. The material is homogeneous, isotropic and linear elastic. Young's modulus, Poisson's ratio and mass density are 199.992 GPa, 0.3 and 5000 kg/m^3, respectively. The tension impact loading $p(t)$ is applied instantaneously to both top and bottom edges with a step function. The load amplitude $p(0)$ is equal to 0.4 GPa, and the time duration is 14 μs. The computed DSIFs are normalized with respect to:

$$K_s = \sigma_0\sqrt{\pi c} \quad (9)$$

where σ_0 is the magnitude of applied stress, c is half of the total crack length. Here, σ_0 is equal to the load amplitude $p(0)$.

Then, Chen's problem is computed using the FE code ABAQUS (2014), in which both the finite element method (FEM) and XFEM are adopted. The simulations are performed with a time step of Δt=0.05 μs. Both 2D (dimensions) and 3D models are compared. Plane strain is assumed in the 2D model. The stress singularity must be considered using contour integral methods for both 2D and 3D FE models. By moving the mid-point nodes to the one-quarter point and keeping the nodes on the cracked face, the singularity effect at the crack front will be included, hence avoiding the use of singular elements in FEM. However, XFEM allows the modeling of the crack geometry independent of the mesh, because it enriches the FE approximation space with special functions that introduce the displacement discontinuity across the crack faces and the singular behaviour associated with the crack front.

Figures 3(b)-(d) show the whole mesh configuration for 2D, 3D FE and 3D XFEM model, respectively. A 6-node quadratic plane strain triangle element (in ABAQUS it is called the CPE6 element) is used to simulate the singularity effect near the crack tip in the 2D model, and 8-node biquadratic plane strain quadrilateral elements (CPE8) are adopted for the other regions of the model. For the 3D model with contour integral method, to simulate the stress singularity, a wedge element (C3D6) is utilized in the region around the crack front, and an 8-node linear brick element (C3D8R) is adopted for the rest of the model. As above, if using the XFEM, the whole 3D model can be discretized with C3D8R elements, and the mesh is regular without singular or highly refined elements at the crack front. For simplicity, the plate thickness of 3D models is divided into 2 elements. The calculations of 2D FE, 3D FE and 3D XFEM model were done in 1'5'', 3'34'' and 4'35'', respectively.

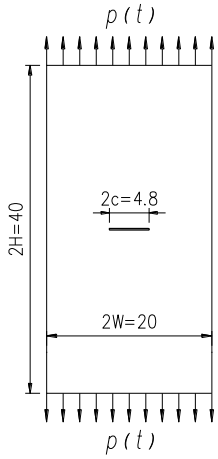

(a) Geometric dimensions and boundary conditions

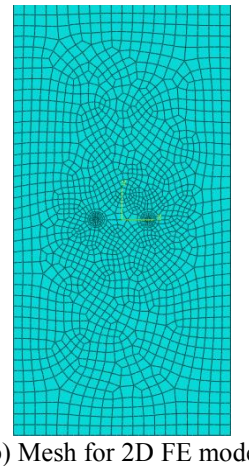

(b) Mesh for 2D FE model

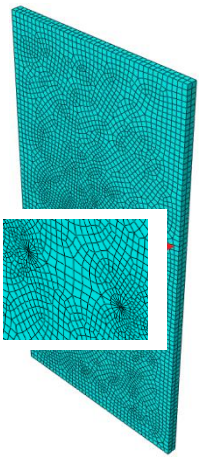

(c) Mesh for 3D FE model

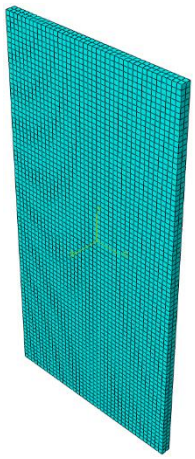

(d) Mesh for 3D XFEM model

Figure 3 CCT specimen

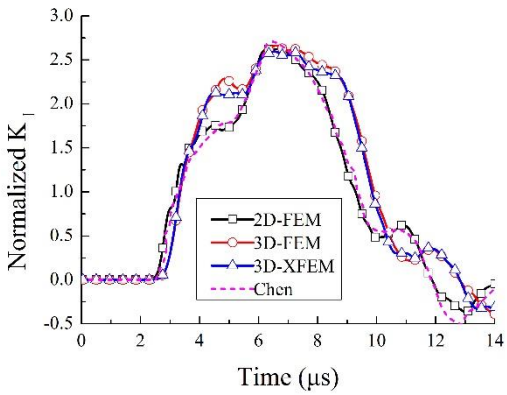

Figure 4 Comparison between the present results and the reference solution by Chen (1975)

The normalized DSIFs by the present methods are compared with those of the reference solution by Chen (1975), as illustrated in Figure 4. It has been noticed that the extractions of $K_I(t)$ from the 3D models are made in the middle layer through the plate thickness. The results of the 2D contour integral method are in good agreement with the reference solution (Chen, 1975) as seen in Figure 4. However, for the 3D models, the numerical results are in general agreement, that is to say, the trend of the DSIFs curves is similar to that of Chen (1975). The main differences are the amplitudes of DSIFs at several points in time. The reason for this is that some differences exist between the 2D and 3D model. For the 3D model, the condition varies from a higher constraint at the middle of the plate to a lower constraint near the free surfaces. Thus, through the 3D model thickness, constraint loss occurs and a plane strain condition will not hold along the crack front. Even so, it is evident that the present numerical results from the 3D models, by means of FEM and XFEM, agree well with each other. The first peak values of them are both higher than Chen's (1975), but the second peak values are quite close. Therefore it can be considered that the XFEM is acceptable for calculating the DSIFs, and that good accuracy can be achieved.

4. FE MODEL FOR CRACKED STIFFENED PLATE

The cracked stiffened plate with a symmetric cross section in Cui *et al*. (2017) has been analysed in the work reported in this paper, as shown in Figure 5. The detailed dimensions of plate and flat-bar stiffener are as follows: plate length a=3400 mm, plate width b=850 mm, plate thickness t_p=22 mm, stiffener height h_w=250 mm and stiffener thickness t_w=25 mm. The stiffener has the same material property as the plate, which is homogeneous, isotropic and linear elastic. The detailed material parameters are as follows: Young's modulus E=205800 MPa, Poisson's ratio v=0.3 and mass density ρ=7800 kg/m^3. The cracked stiffened plate is subjected to tension step load $p(t)$ on the transverse edge, with duration t_d=2.5 ms and load peak $p(0)$=50 MPa. The crack with a length $2c$=250 mm is located in the middle of the plate and is symmetric with respect to the stiffener.

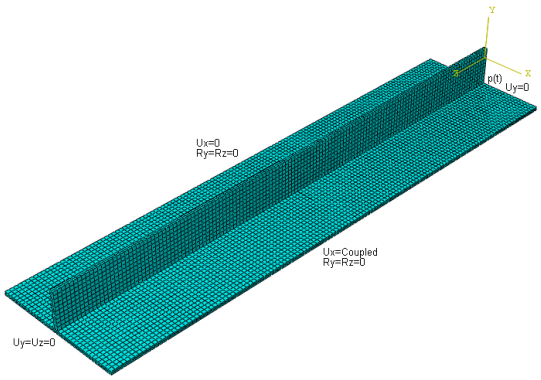

(a) Boundary and loading conditions for 3D XFEM model

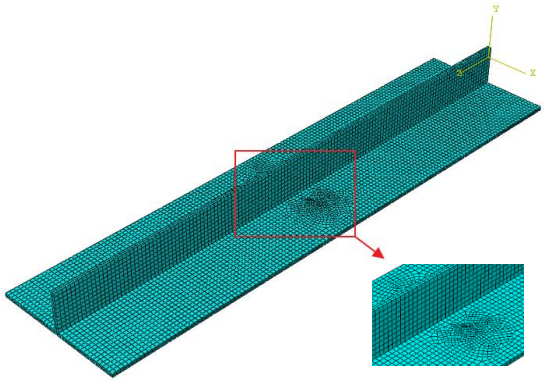

(b) Mesh for 3D FE model

Figure 5 Cracked stiffened plate

As the model in the present study is a combination of one stiffener with attached plate, which is extracted out of a continuous plated structure, such as the deck of a ship hull girder, proper boundary and loading conditions have to be imposed in order to simulate real behaviour of a ship's stiffened plate. Figure 5(a) depicts the boundary/loading conditions of the cracked stiffened plate model. Longitudinal edges of the cracked stiffened plate are assumed to have symmetrical conditions. Moreover, the tension impact loading is applied on the simply-supported straight loaded edge, while its opposite simply-supported unloaded edge is restrained against in-plane movement.

For the XFEM model, the FE code ABAQUS cannot properly define the crack if the symmetry plane lies on the crack plane. Thus, the z-plane (crack plane) symmetry is not used. The 8-node C3D8R element has been selected to discretize the whole stiffened plate model. Then the XFEM mesh, as shown in Figure 5(a), is built with a regular linear hexahedrons 3D grid. In the XFEM simulations, a time step Δt=0.02 ms and an average mesh size 25 mm are employed, except that the number of elements along the plate and web thickness direction is specified to be 2. The XFEM calculation was done in 3'34''.

In order to further verify the reliability of DSIFs by using XFEM, the 3D contour integral method has been adopted to calculate the model again. Then, to simulate the stress singularity, a wedge C3D6 element was used in the region around the crack front, and C3D8R element adopted for the rest of the model. The whole mesh configuration for the 3D FE model is shown in Figure 5(b). Keeping boundary/loading conditions and other calculating parameters the same as XFEM model, the FE calculation was done in 2'17''. Figure 6 presents a comparison between the numerical results by XFEM and 3D contour integral method. As mentioned in Section 3, the middle layer node at the crack front was chosen to extract $K_I(t)$ for the present stiffened plate model. The abscissa indicates time. The ordinate indicates the mode I DSIFs normalized with respect to K_s given by Eq. (9). It is seen that $K_I(t)$ from two different methods are almost identical, except that the result of XFEM is slightly higher than that of 3D contour integral method. The advantage of XFEM is shown that discontinuities can be modeled within elements through the enrichment of discontinuous shape functions, and the discontinuous fields can be illustrated in regular meshes without the use of singular elements at the crack front. Therefore, it can be concluded that both accuracy and performance of XFEM are excellent, and there is less than 2% variation between the results of FEM and XFEM.

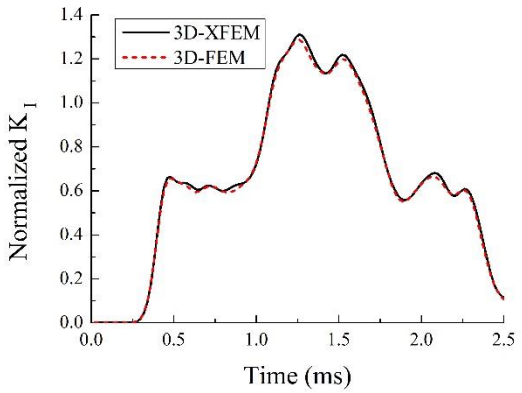

Figure 6 Normalized $K_I(t)$ by two different methods

4.1 MESH SENSITIVITY ANALYSIS

To simulate the stress singularity at the crack tip, meshes have to be refined locally using classical finite element method (FEM). However, because of the introduction of the displacement field approximation, good results can be obtained with coarser meshes using XFEM. In order to determine the best size of elements based on a compromise between computational cost and accuracy, three types of mesh generations have been considered for the cracked stiffened plate model shown in Figure 5(a). The detailed mesh sizes and total number of elements are described in Table 1. Figure 7 illustrates the comparison of the normalized $K_I(t)$ at the middle layer node of the crack front. It can be seen that with the refinement of mesh, the magnitude of $K_I(t)$ decreases and appears to converge. As a result, for the present model, a convergence solution can be achieved with moderate refinement, i.e., average mesh size 25 mm.

Table 1 Mesh sizes and number of elements

Case	Element size along longitudinal edges (mm)	Element size along transverse edges (mm)	Element size of stiffener web (mm)	Total number of elements
Coarse mesh	50	25	25	6256
Moderate mesh	25	25	25	12512
Fine mesh	25	12.5	25	21216

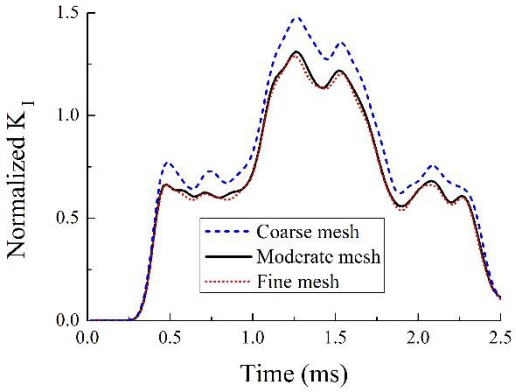

Figure 7 Normalized $\boldsymbol{K_I(t)}$ for different mesh sizes

4.2 TIME STEP SENSITIVITY ANALYSIS

For step loading, transient DSIFs are highly influenced by the choice of time step increment, because the waves induced by this loading have a significant influence on crack tip fields (Song & Paulino, 2006). Here, three different time steps, 0.01 ms, 0.02 ms and 0.05 ms, were chosen to investigate the influence of time step on the DSIFs. As expected, numerical results were highly influenced by the time step, which can be seen in Figure 8. As the time step decreases, the numerical results appear to converge. For the larger time step, such as Δt=0.05 ms, the magnitude of $K_I(t)$ is influenced, and the maximum relative error is close to 13%. Besides, the variation of normalized DSIFs versus time is obviously different near the peaks. For the present model, a convergence solution can be obtained with a time step Δt=0.02 ms.

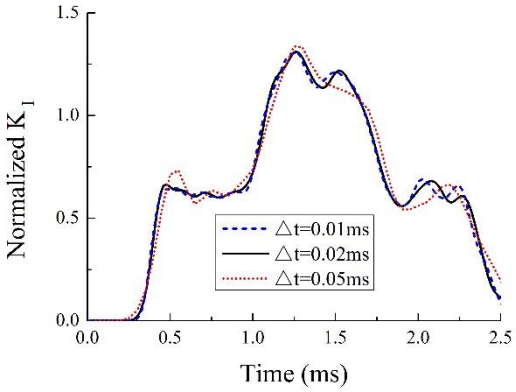

Figure 8 Normalized $K_I(t)$ for different time steps

5. DISCUSSIONS OF INFLUENTIAL PARAMETERS

In this section, a series of numerical analyses are reported in investigating DSIFs for stiffened plates with a mode I crack shown in Figure 5(a). The influence of different parameters on the variation of DSIFs is discussed, such as stiffener height, the longitudinal location and length of cracks. Unless specifically indicated, only a single parameter is varied in each case.

5.1 INFLUENCE OF STIFFENER HEIGHT

In a stiffened plate where the stiffeners are attached to the plate by means of welding, once a crack reaches a stiffener, the crack may propagate into and completely sever the stiffener from the plate. Since DSIFs are important fracture characterizing parameters, it is necessary to check the effect of stiffener height on the DSIFs of such cracked stiffened plates. Three kinds of stiffener height (h_w=200 mm, 250 mm, 300 mm) were selected, while the crack longitudinal location fixed at the middle span. In addition, the crack length was kept constant at 250 mm. Figure 9 shows the normalized $K_I(t)$ at the middle layer node of the crack front with different stiffener heights. It can be seen that the peak of $K_I(t)$ decreases as the stiffener height increases, and the time to reach peak value delays gradually. The first peak value for the case when h_w=300 mm was found to be 18.1% less than the case when h_w=200 mm, and the second peak value was reduced by 10.4%. This result indicates that the stiffener can effectively reduce the near crack-tip stress field, which is very beneficial in studying the terminating of crack propagation.

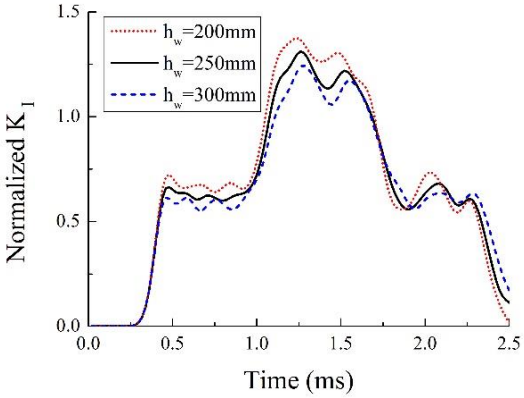

Figure 9 Normalized $K_I(t)$ for different stiffener heights

Figure 10 illustrates the von-Mises stress distributions at different times for cracked models with varying stiffener heights. As can be seen, the highly stressed region of the stiffener increased gradually with the increase of stiffener height, and the crack opening width decreased accordingly. This result is consistent with that from $K_I(t)$. Therefore, the proper application of stiffeners is seen to be a future research topic.

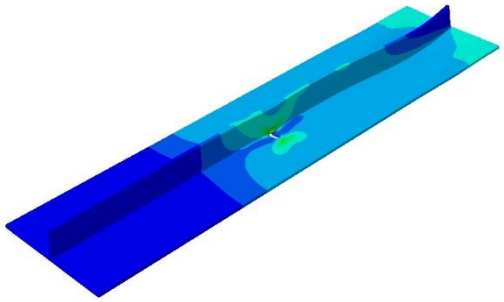

(a) Time=0.48 ms, h_w=200 mm

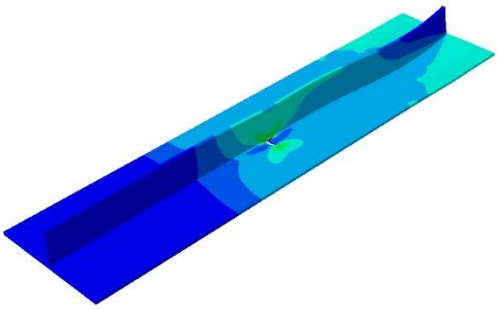

(b) Time=0.48 ms, h_w=250 mm

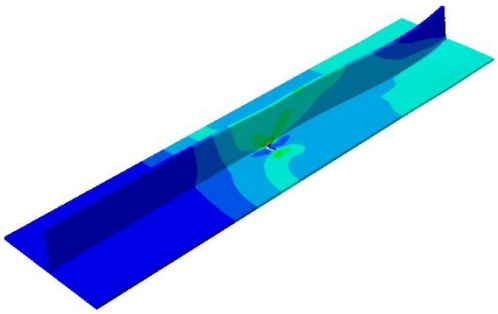

(c) Time=0.48 ms, h_w=300 mm

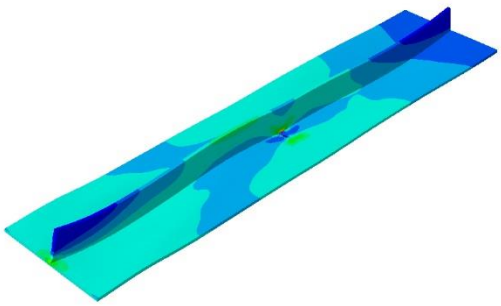

(d) Time=1.26 ms, h_w=200 mm

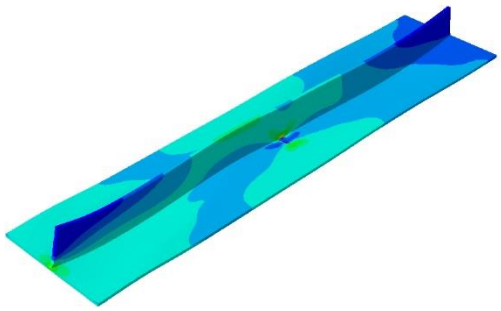

(e) Time=1.26 ms, h_w=250 mm

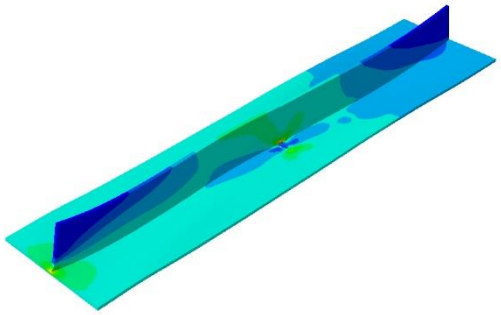

(f) Time=1.26 ms, h_w=300 mm

Figure 10 Von-Mises stress distributions at different times for cracked models with varying stiffener heights

5.2 INFLUENCE OF CRACK LOCATION

In order to examine the influence of crack location on the DSIFs, the ratio of crack longitudinal location to plate length (s/a) was altered in the range of 2/8-4/8, while the crack transverse location kept unchanged. When s/a=4/8, the crack was located in the middle span of stiffened plate. With the crack length fixed at 250 mm, Figure 11 shows the normalized $K_I(t)$ for different crack longitudinal locations. When the crack moved towards the unloaded edge of stiffened plate, the distance between the impact load and the crack tip became longer, and the time of stress wave reaching the crack tip delayed accordingly. Thus the numerical initiation time and the first peak time were also delayed, as indicated in Figure 11. The magnitude of first peak was slightly influenced by the crack longitudinal location, with the maximum difference less than 4.4%, and the oscillation in $K_I(t)$ was weakened. The second peak value of $K_I(t)$ and the corresponding time of reaching it decreased, while the oscillation was enhanced. This was mainly due to the interaction between the stress wave and reflected wave, which was generated when the stress wave reached the crack surfaces or geometric boundaries. When the crack moved to the middle span, a reduction in the second peak value of 5.6% was estimated in comparison to the case when s/a=2/8.

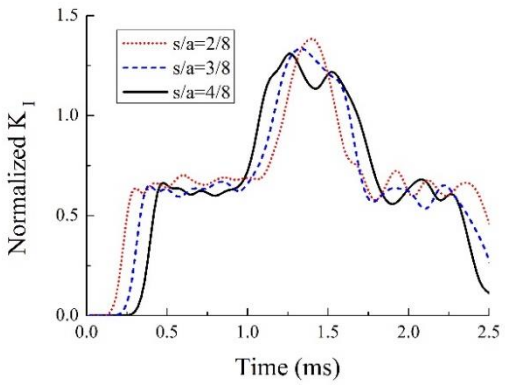

Figure 11 Normalized $K_I(t)$ for different crack locations

Figure 12 shows the von-Mises stress distributions at different times for cracked models with varying crack locations. It can be seen that the stress distributions of cracked stiffened plates were affected by the crack location obviously. When moving the crack in the longitudinal direction, the highly stressed region of stiffened plate was moved accordingly, and the crack opening or closure was different.

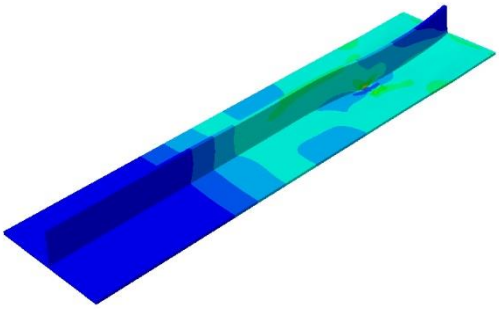

(a) Time=0.48 ms, *s/a*=2/8

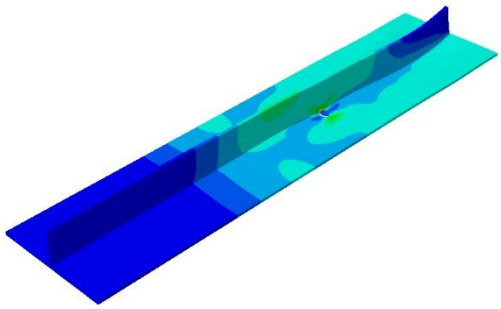

(b) Time=0.48 ms, *s/a*=3/8

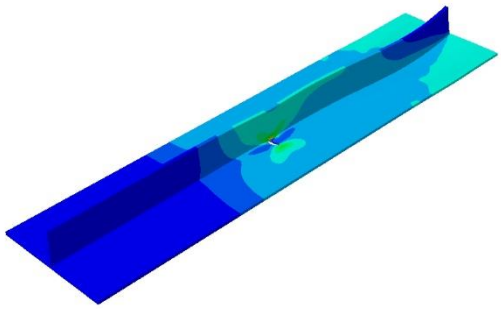

(c) Time=0.48 ms, *s/a*=4/8

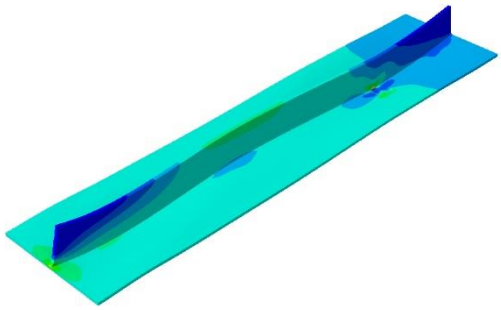

(d) Time=1.26 ms, *s/a*=2/8

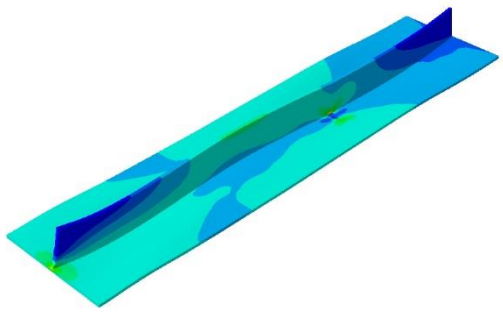

(e) Time=1.26 ms, *s/a*=3/8

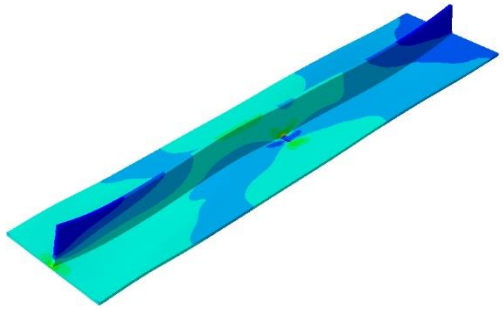

(f) Time=1.26 ms, *s/a*=4/8

Figure 12 Von-Mises stress distributions at different times for cracked models with varying crack locations

5.3 INFLUENCE OF CRACK LENGTH

In order to investigate the effect of crack length on the mode I DSIFs of stiffened plates, the case with stiffener height h_w=250 mm having crack location *s*/*a*= 4/8 was considered, while the crack length in the plate was varied. Figure 13 presents the normalized $K_I(t)$ at the middle layer node of the crack front with three different crack lengths (2*c*=150 mm, 250 mm, 350 mm). Compared to the stiffener height and crack location, the variation of crack length slightly affected the mode I DSIFs with the difference less than 3%, as illustrated in Figure 13. Even so, the magnitude of $K_I(t)$ increased as the length of crack increased, and the time of reaching peak value delayed gradually. This indicated that the near crack-tip stress field was enhanced when the crack length became longer. But, due to the restraint of stiffener, the mode I DSIFs were not very sensitive to the variation of crack length for stiffened plate models with central crack located only in the plate.

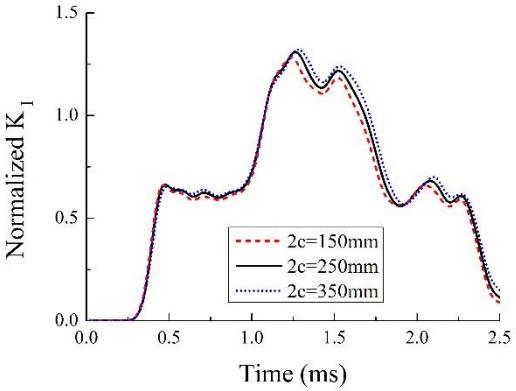

Figure 13 Normalized $K_I(t)$ for different crack lengths

Figure 14 shows the von-Mises stress distributions at different times for cracked models with varying crack lengths. It can be seen that the stress distributions of the three cracked models are obviously different. As the crack length became longer, the stress was concentrated in the vicinity of cracking damage, and the crack opening width increased gradually.

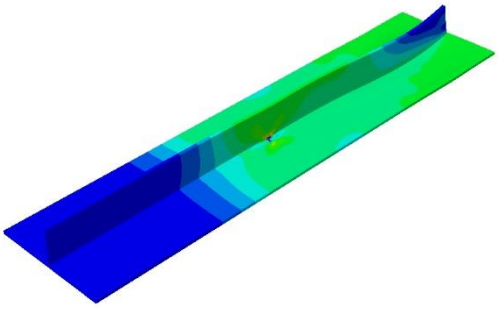

(a) Time=0.48 ms, 2c=150 mm

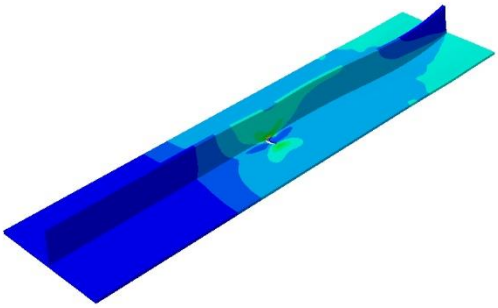

(b) Time=0.48 ms, 2c=250 mm

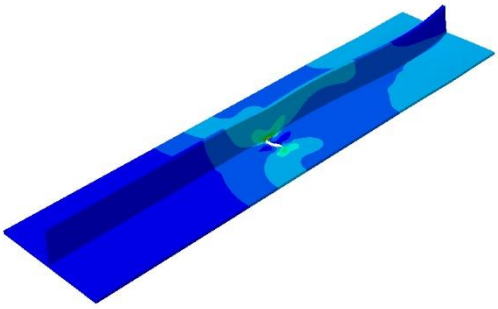

(c) Time=0.48 ms, 2c=350 mm

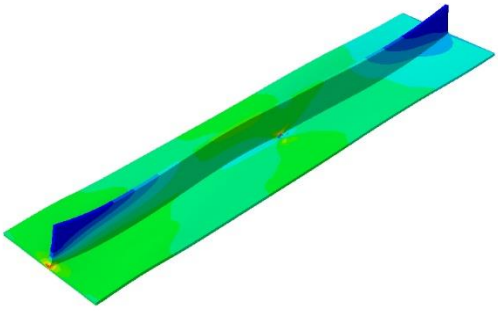

(d) Time=1.26 ms, 2c=150 mm

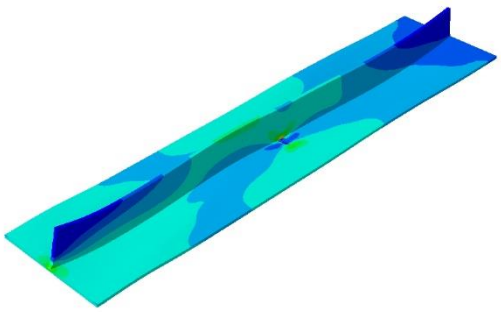

(e) Time=1.26 ms, 2c=250 mm

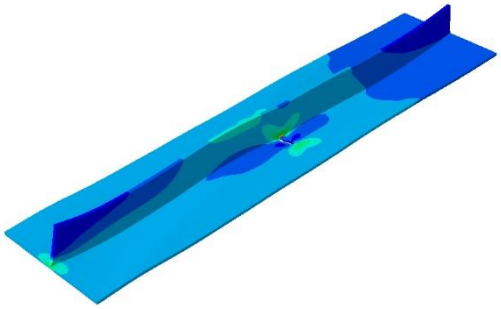

(f) Time=1.26 ms, 2c=350 mm

Figure 14 Von-Mises stress distributions at different times for cracked models with varying crack lengths

6. CONCLUSIONS

Dynamic fracture behaviour for stiffened plates subjected to tension impact loading is numerically studied in this paper. A series of FE simulations were performed by means of XFEM using ABAQUS. The actual boundary conditions of cracked stiffened plates in ship structures have been considered. The influences of crack length and longitudinal location, as well as stiffener height, on the DSIFs have been investigated. Based on these results in the present study, the major conclusions can be summarised as follows:

1) The crack can be modeled within elements by XFEM, and XFEM makes its analysis, to some extent, independent of the mesh. The results by XFEM are reasonable, with the error less than 2% in contrast to those by FEM.
2) As the stiffener height increases, the peak of mode I DSIFs decreases due to the restraint of stiffener, and the time to reach peak value is gradually delayed. The maximum reduction in peak values is estimated to be 18.1%.
3) The longitudinal location of crack has a significant influence on the DSIFs. As the crack moves towards the middle span, the first peak value is slightly influenced, with the maximum difference less than 4.4%, and the oscillation in $K_I(t)$ is weakened. The second peak value is reduced by 5.6%, while the oscillation is enhanced.
4) The mode I DSIFs are not very sensitive to the variation of crack length for stiffened plates if the crack is centrally located in the plate.

5) It is evident that the mesh size and time step affect the numerical results. To obtain the convergence solutions, moderate meshes and time steps should be chosen reasonably, such as an average mesh 25 mm and a time step 0.02 ms for the present model.

Due to complexity involved in the dynamic analysis, the derived results are limited to cases studied in this paper, which may not be directly extended to other cases with different material properties, load types or boundary conditions.

7. ACKNOWLEDGEMENTS

The authors are grateful for the financial support from the National Natural Science Foundation of China (Grant No. 51779198).

8. REFERENCES

1. *ABAQUS User's Manual Version 6.14* (2014). Dassault Systémes Simulia Corporation, Providence, RI.
2. AGARWAL, P., CHAKRABORTY, A. and SINGH, A. (2015) *Simulation of bi-material plate by XFEM under dynamic load*. Materials Today: Proceedings, 2(4-5), pp. 1552-1559. DOI: 10.1016/j.matpr.2015.07.081
3. BELYTSCHKO, T. and BLACK, T. (1999) *Elastic crack growth in finite elements with minimal remeshing*. International Journal for Numerical Methods in Engineering, 45, pp. 601-620. DOI: 10.1002/(sici)1097-0207 (19990620)45:5<601::aid-nme598>3.0.co;2-s
4. BERGARA, A., DORADO, J.I., MARTIN-MEIZOSO, A. and MARTÍNEZ-ESNAOLA, J.M. (2017) *Fatigue crack propagation in complex stress fields: Experiments and numerical simulations using the Extended Finite Element Method (XFEM)*. International Journal of Fatigue, 103, pp. 112-121. DOI: 10.1016/j.ijfatigue.2017.05.026
5. CHEN, G.H. and CHEN, L.J. (2013) *Dynamic fracture research based on XFEM and its application on discharge valve guard of hydrogen compressor*. Engineering Failure Analysis, 34, pp. 59-68. DOI: 10.1016/j.engfailanal.2013.07.002
6. CHEN, Y.M. (1975) *Numerical computation of dynamic stress intensity factors by a Lagrangian finite-difference method (the HEMP code)*. Engineering Fracture Mechanics, 7(4), pp. 653-660. DOI: 10.1016/0013-7944(75)90021-1
7. CUI, C., YANG, P., LI, C. and XIA, T. (2017) *Ultimate strength characteristics of cracked stiffened plates subjected to uniaxial compression*. Thin-Walled Structures, 113, pp. 27-38. DOI: 10.1016/j.tws.2017.01.003
8. DOLBOW, J., MOËS, N. and BELYTSCHKO, T. (2000) *Discontinuous enrichment in finite elements with a partition of unity method*. Finite Elements in Analysis and Design, 36, pp. 235-260. DOI: 10.1016/s0168-874x(00)00035-4
9. FENG, S.Z. and LI, W. (2018) *An accurate and efficient algorithm for the simulation of fatigue crack growth based on XFEM and combined approximations*. Applied Mathematical Modelling, 55, pp. 600-615. DOI: 10.1016/ j.apm.2017.11.015
10. GONZÁLEZ-ALBUIXECH, V.F., GINER, E., TARANCÓN, J.E., FUENMAYOR, F.J. and GRAVOUIL, A. (2013) *Convergence of domain integrals for stress intensity factor extraction in 2-D curved cracks problems with the extended finite element method*. International Journal for Numerical Methods in Engineering, 94, pp. 740-757. DOI: 10.1002/nme.4478
11. GONZÁLEZ-ALBUIXECH, V.F., GINER, E., TARANCÓN, J.E., FUENMAYOR, F.J. and GRAVOUIL, A. (2013) *Domain integral formulation for 3-D curved and non-planar cracks with the extended finite element method*. Computer Methods in Applied Mechanics and Engineering, 264, pp. 129-144. DOI: 10.1016/j.cma.2013.05.016
12. HABOUSSA, D., GRÉGOIRE, D., ELGUEDJ, T., MAIGRE, H. and COMBESCURE, A. (2011) *X-FEM analysis of the effects of holes or other cracks on dynamic crack propagations*. International Journal for Numerical Methods in Engineering, 86, pp. 618-636. DOI: 10.1002/nme.3128
13. KUMAR, M., BHUWAL, A.S., SINGH, I.V., MISHRA, B.K., AHMAD, S., RAO, A.V. and KUMAR, V. (2017) *Nonlinear fatigue crack growth simulations using J-integral decomposition and XFEM*. Procedia Engineering, 173, pp. 1209-1214. DOI: 10.1016/j.proeng.2016.12.126
14. LIN, X. and BALLMANN, J. (1993) *Re-consideration of Chen's problem by finite difference method*. Engineering Fracture Mechanics, 44(5), pp. 735-739. DOI: 10.1016/0013-7944(93)90202-4
15. MENOUILLARD, T., SONG, J.H., DUAN, Q. and BELYTSCHKO, T. (2010) *Time dependent crack tip enrichment for dynamic crack propagation*. International Journal of Fatigue, 162 (1-2), pp. 33-49. DOI: 10.1007/s10704-009-9405-9
16. MOËS, N., DOLBOW, J. and BELYTSCHKO, T. (1999) *A finite element method for crack growth without remeshing*. International Journal for Numerical Methods in Engineering, 46, pp. 131-150. DOI: 10.1002/ (sici)1097-0207 (19990910)46:1<131::aid-nme726>3.0.co;2-j
17. NISTOR, I., PANTALÉ, O. and CAPERAA, S. (2008) *Numerical implementation of the*

eXtended Finite Element Method for dynamic crack analysis. Advances in Engineering Software, 39, pp. 573-587. DOI: 10.1016/j.advengsoft.2007.06.003

18. QIAN, G., GONZÁLEZ-ALBUIXECH, V.F., NIFFENEGGER, M. and GINER, E. (2016) *Comparison of K_I calculation methods*. Engineering Fracture Mechanics, 156, pp. 52-67. DOI: 10.1016/j.engfracmech.2016.02.014
19. SARIBAY, M. and NIED, H.F. (2014) *Dynamic stress intensity factors for suddenly loaded structures using enriched finite element*. Theoretical and Applied Fracture Mechanics, 70, pp. 59-67. DOI: 10.1016/j.tafmec.2014.02.003
20. SHIMBO, T. (2017) *Development and application of a dynamic XFEM for the seismic residual displacement analysis of an embankment*. Soils and Foundations, 57(3), pp. 357-370. DOI: 10.1016/j.sandf.2017.05.004
21. SONG, S.H. and PAULINO, G.H. (2006) *Dynamic stress intensity factors for homogeneous and smoothly heterogeneous materials using the interaction integral method*. International Journal of Solids and Structures, 43(16), pp. 4830-4866. DOI: 10.1016 /j.ijsolstr.2005.06.102
22. SUKUMAR, N., MOËS, N., MORAN, B. and BELYTSCHKO, T. (2000) *Extended finite element method for three-dimensional crack modelling*. International Journal for Numerical Methods in Engineering, 48, pp. 1549-1570. DOI: 10.1002/1097-0207(20000820) 48:11<1549::aid-nme955>3.0.co;2-a
23. WANG, Y.X., CERIGATO, C., WAISMAN, H. and BENVENUTI, E. (2017) *XFEM with high-order material-dependent enrichment functions for stress intensity factors calculation of interface cracks using Irwin's crack closure integral*. Engineering Fracture Mechanics, 178, pp. 148-168. DOI: 10.1016/ j.engfracmech.2017.04.021
24. WEN, L.F. and TIAN, R. (2016) *Improved XFEM: Accurate and robust dynamic crack growth simulation*. Computer methods in applied mechanics and engineering, 308, pp. 256-285. DOI: 10.1016/j.cma.2016.05.013
25. XIE, D. and BIGGERS JR., S.B. (2007) *Calculation of transient strain energy release rates under impact loading based on the virtual crack closure technique*. International Journal of Impact Engineering, 34(6), pp. 1047-1060. DOI: 10.1016/j.ijimpeng.2006.02.007
26. XIE, D., QIAN, Q. and LI, C.A. (2009) *Numerical Calculation Method of Fracture Mechanics and Engineering Application*. Science Press, Beijing, pp. 135-137. ISBN 978-7-03-025167-1 (in Chinese)

